Unveiling Unprecedented Facet of Mg Batteries: Ultrahigh Power

Hui Dong[1]†, Oscar Tutusaus[2]†, Yanliang Liang[1,3], Ye Zhang[1], Zachary Lebens-Higgins[4,5], Wanli Yang[5], Rana Mohtadi[2]*, Yan Yao[1,3]*

[1]Department of Electrical and Computer Engineering and Materials Science and Engineering Program, University of Houston, Houston, TX 77204, USA

[2]Materials Research Department, Toyota Research Institute of North America, Ann Arbor, MI 48105, USA

[3]Texas Center for Superconductivity, University of Houston, Houston, TX 77204, USA

[4]Department of Physics, Applied Physics and Astronomy, Binghamton University, Binghamton, NY 13902, USA

[5]Advanced Light Source, Lawrence Berkeley National Laboratory, 1 Cyclotron Road, Berkeley, CA 94720, USA

†These authors contributed equally: Hui Dong, Oscar Tutusaus

*Correspondence author. Email: rana.mohtadi@toyota.com, yyao4@uh.edu

Abstract: Magnesium batteries have long been pursued as potentially high-energy and safe alternatives to Li-ion batteries; however, fast charge-discharge capability, one of the most desired properties for advanced batteries, remains elusive for this technology. Here, we develop a next generation Mg battery prototype, delivering a specific energy of up to 566 Wh kg^{-1} and an ultrahigh specific power of up to 30.4 kW kg^{-1}, which is close to two orders of magnitude higher than state-of-the-art Mg battery. This is achieved by coupling a kinetically fast organic cathode material, operating under bond cleavage-free solid-liquid reaction, and an electrolyte capable of providing dendrite-free Mg deposition-stripping at a record current density of 20 mA cm^{-2}.

One Sentence Summary: Ultrahigh power, an unprecedented quality of Mg battery, is unveiled and demonstrated using a prototype combining a quinone-based cathode and a second to none $Mg(CB_{11}H_{12})_2$ electrolyte that enables ultrahigh rate cycling of dendrite-free Mg anode.

Main Text:

The rapid growth and adoption of electrochemical energy storage in our society calls for developing next-generation batteries that combine high energy, high power, and low cost. Among many post-lithium-ion batteries (*1-3*), rechargeable magnesium batteries utilizing divalent Mg^{2+} as charge carriers are expected to offer significant improvements in volumetric energy density and affordability of batteries due to the use of earth-abundant, high-capacity, and dendrite-free (safe) Mg metal anode (*1, 4, 5*). However, power density has been the Achilles' heel for this technology. The root cause of this challenge stems from the divalent Mg^{2+} ion: it holds twice the amount of charge of Li^+, whilst having a similar ionic radius. This high charge density results in strong interactions with electrolyte solution species (i.e. solvent, anion) and lattice atoms of cathode materials. As a result, ion dissociation from electrolyte complexes and ionic solid-state diffusion, two essential processes in classical intercalation chemistry, are

sluggish at room temperature (*6-8*). Even the most efficient intercalation-type cathode materials such as Mo_6S_8 require elevated temperature to approach their theoretical capacity (*1*). Other insertion-type cathode materials that show fast kinetics at room temperature, notably organic polymers and layered compounds, have been found to actually store partially complex ions such as $MgCl^+$ and solvated ions (*9-11*). While the storage of complex ions circumvents the dissociation and diffusion difficulties associated with Mg^{2+}, it also brings new challenges: limited cycle life caused by volume changes in the electrode (i.e. due to co-insertion of bulky solvent molecules) or reduced practical cell-level energy density caused by its function as a hybrid battery (*9, 12*). A strategy to overcome the challenges of ionic dissociation and solid-state diffusion, whilst solely storing Mg^{2+} (instead of its complex forms), is through solid-liquid reactions. In this case, a solid cathode material is converted to partially soluble intermediates before precipitating into a solid product. Examples include conversion-type cathode materials such as sulfur: both sulfur and the corresponding discharged product MgS are insoluble while the polysulfide intermediates are soluble (*13-15*). However, these materials still display slow kinetics partially due to the electrochemically irreversible bond cleavage and re-formation involved in the reactions (*15-17*). Cathode materials that can support fast Mg^{2+} storage would therefore require a new electrode reaction mechanism.

Electrolyte design also plays a crucial role in improving battery kinetics. Historically, Mg electrolyte solutions hinged on the presence of chloride to increase salt solubility and reversible Mg deposition-stripping (*18*). While those remain in the mainstream, efficient chloride-free electrolyte solutions have recently been discovered arising for a need to overcome serious challenges associated with chlorides, such as corrosion of current collectors and high dissociation energy of Mg-Cl bond (*18-20*). We contributed to this new direction with the development of the boron cluster-based Mg electrolyte, $Mg(CB_{11}H_{12})_2$ (MMC), which was later recognized as a breakthrough in Mg electrolytes (*2, 19*). MMC dissolves in oligomeric solvents such as triglyme (G3) and tetraglyme (G4) to form some of the best performing Mg electrolyte solutions in terms of reversibility of Mg deposition/stripping, electrochemical window, water stability, and non-corrosivity (*19*). Two important shortcomings of higher glyme solvents are their high viscosity and their strong coordinating ability, which are responsible for hindering ionic motion and slow kinetics at the electrolyte-electrode interface (*21, 22*). Lower-weight ether solvents, on the other hand, struggle to dissolve MMC (*19*). A suitable solvent capable of fast ion conduction without compromising salt solubility remains a critical missing piece towards a fast kinetic Mg battery.

Here we report a high-power Mg battery that can be charged-discharged at up to 20 A g^{-1} and deliver a specific power of 30.4 kW kg^{-1}, close to two orders of magnitude higher than the second highest power Mg battery (0.44 kW kg^{-1}) (table S1). This prototype is made possible through coupling an organic cathode material, pyrene-4,5,9,10-tetraone (PTO), with a modified MMC electrolyte solution. PTO undergoes a solid-liquid reaction that does not involve chemical bond cleavage-re-formation, thus providing fast redox kinetics. A high specific capacity of 315 mAh g^{-1} is recorded for PTO at a respectable voltage of 2.1 V vs Mg^{2+}/Mg. The modified MMC electrolyte solution utilizes a unique solvent blend, which simultaneously enables fast ion motion and high MMC solubility. Unprecedented high-rate of Mg plating in a dendrite-free fashion at a current density of 20 mA cm^{-2} and areal capacity of 3 mAh cm^{-2} has been realized. Our results set

a new precedent for ultrahigh rate cycling of energy-dense metals and offer a new thrust towards research on Mg metal batteries.

PTO was selected as cathode material owing to its high theoretical specific capacity (408 mAh g^{-1}) and storage of solvent-free Mg^{2+} (fig. S1). The electrochemical behavior of PTO was first evaluated in a two-electrode Mg-PTO Swagelok cell using an MMC/G4 electrolyte. Fig. 1A shows a typical voltage profile with two discharge plateaus corresponding to two 2-electron reductions, in agreement with the four carbonyl groups in a PTO molecule (C=O ⇔ C–O^-). Synchrotron-based soft X-ray absorption spectroscopy (sXAS) confirms the electrochemical reactions of carbonyl groups are indeed reversible (fig. S2A). The observed specific capacity of 315 mAh g^{-1} and average discharge voltage of 2.03 V represent one of the highest reported values for Mg batteries. X-ray photoelectron spectroscopy (XPS) and inductively coupled plasma optical emission spectroscopy (ICP-OES) measurements of discharged PTO electrodes reveal low atomic ratios of B:Mg of 2.12 and 2.54, respectively (fig. S2B). The results indicate that Mg^{2+}, rather than the anion-bound $Mg(CB_{11}H_{12})^+$ which has a ratio of 11:1, is the main stored species. This important evidence promoted us to further study this cathode-electrolyte combination.

The solid-liquid reaction mechanism of PTO was validated by optical characterizations. PTO electrodes at different states of discharge were extracted from the Swagelok cells and submerged in 1,2-dimethoxyethane (DME) solvent for three minutes. A half-discharged (2.0 V) electrode gives a deep purple solution (inset of Fig. 1A), indicating a soluble reaction intermediate. A fully discharged (0.9 V) electrode gives a colorless solution, suggesting the final discharge product Mg_2PTO is insoluble. The reduction of PTO can therefore be described as a solid-liquid reaction: the solid PTO is reduced to a proposed soluble Mg_1PTO intermediate (fig. S3A), then to the insoluble Mg_2PTO as the final product. While the solid-liquid reaction of PTO resembles that of sulfur, a key difference manifests in that no bond cleavage-re-formation is involved in the enolization reduction (C=O ⇔ C–O^-) of PTO. To compare the intrinsic kinetic difference at molecular level, we probed the electrochemical properties of dissolved PTO molecules in a 0.1M tetra-*n*-butylammonium perchlorate solution in acetonitrile due to its solubility, low-viscosity and high-conductivity, and compared with that of sulfur (S_8) molecules. In cyclic voltammetry (CV), peak potential separation (*ΔE*) between a pair of reduction and oxidation peaks is informative of the electrochemical reversibility and reaction kinetics (*23*). For a PTO molecule, four sequential one-electron reduction peaks, corresponding to reducing four C=O groups, take place (Fig. 1B). *ΔE* of these peaks range from 65 to 92 mV (table S3), confirming high reversibility and intrinsically fast kinetics (*24, 25*). In contrast, two 2-electron redox peaks for S_8, attributed to S_8 ⇔ S_8^{2-} and S_8^{2-} → $2S_4^{2-}$, occur (Fig.1C) (*26*); *ΔE* of the first and second reduction peaks are 259 and 83 mV, respectively, reflecting much slower kinetics of S_8 than that of PTO. Further, the maximum reduction of S_8 during solution CV measurements is 4 e^-/S_8 (*26*), significantly lower than the 12-16 e^-/S_8 observed from a long-term galvanostatic discharge of a solid electrode, while PTO shows 4 e^- /PTO in both cases. Notably, the kinetic advantage of PTO is also observed at the electrode level (Fig.1D), where the specific capacities of a PTO electrode in a battery cell at 0.2 C, 1 C, and 5 C are 315, 288, and 176 mAh g^{-1}, respectively. This translates to a power density of 3363 W kg^{-1} at 5 C, surpassing the previous state-of-art power performance of Mg-S (441 W kg^{-1}) and Mg-Mo_6S_8 (270 W kg^{-1} at 50 °C).

With a soluble reaction intermediate comes two concerns familiar with other solid-liquid reaction-based batteries: cathode material loss caused by continued dissolution upon cycling and passivation of the metal anode by the dissolved cathode species. Both concerns were effectively placed under control in our system. Even though the PTO electrode does decay fast if the dissolution of PTO is left unattended (fig. S3B), the decay has been efficiently mitigated by insertion of a thin (~2 μm) and light-weight (0.48 mg cm^{-2}) graphene oxide (GO) membrane (fig. S4, A and B) between the cathode and the separator to trap the intermediate (Fig. 2A), an approach proven effective for Li-S batteries (*27*). After including a GO membrane, the reversible capacity reaches 315 mAh g^{-1} following an initial activation step and stabilize for another 500 cycles with a capacity retention of 84% (Fig. 2B). Note that the GO membrane (and the conductive carbon in the PTO electrode) has negligible contribution to the cathode capacity (Fig. S6). On the other hand, the passivation of Mg anode does not seem to apply to Mg-PTO batteries, despite being a known issue for Mg-S batteries caused by the trace amounts of dissolved polysulfides in the electrolyte solution (*28*). We have investigated Mg plating behavior in MMC/G4 electrolyte solutions with and without dissolved Mg_1PTO intermediate and found no significant variation in the overpotentials for deposition-stripping (Fig. 2C and fig. S7A). XPS characterization of anode surface (fig. S7B) shows signature of Mg_2PTO products, but its presence did not negatively affect the Mg deposition/stripping process (fig. S7D). This behavior contrasts with that in MMC/G4 electrolyte solutions containing soluble MgS_8 intermediate, where the overpotential almost doubled (Fig. 2D and fig. S7C), in agreement with previous reports (*28*).

While the fast kinetics of PTO cathode are demonstrated in our Mg-PTO cell, the cell power is still limited by the slow mass transport in the MMC/G4 electrolyte solution. We sought to exploit the full power capabilities of PTO cathode by employing solvents that are less viscous and less coordinating than G4. Although many short-chain ethers meet these requirements, MMC has been found to have poor solubility in these solvents (*19*). We have therefore explored solvent blends, a common practice in Li-ion battery electrolyte development, but still very infrequent in Mg battery research. A screening of ethereal solvent combinations (see Methods) revealed a cooperative effect between a narrow group of candidates that enable solubilization of MMC (Fig. 3A). Optimization of ionic conductivity within the available solubility space yields 0.5 *m* MMC in 1,2-dimethoxyethane/diglyme (DME/G2) (1:1) [MMC/(DME-G2)] as a superior candidate to MMC/G4 (Fig. 3, B and C; fig. S8, A, B and C), with an improved ionic conductivity of 6.1 mS cm^{-1} at 25°C. A mixed-solvent-shell of Mg^{2+} ions is observed in this electrolyte (see Supplementary Text) (*29*).

The modified electrolyte solution MMC/(DME-G2) significantly improves the kinetics of Mg anode without compromising its coulombic efficiency (CE). Following a method developed for Li metal (*30*) to accurately determine CE in a Mg|Cu asymmetric cell, we confirmed an exceptional CE of 99.9% for MMC/(DME-G2) (fig. S8D and Methods). Cyclic voltammetry of MMC/(DME-G2) in a three-electrode setup using Pt disk as the working electrode reveals a low overpotential (<250 mV) for Mg plating similar to that of MMC/G4. Of particular interest is that very high current densities are observed for Mg stripping, approaching 100 mA cm^{-2}, an order of magnitude higher than that for MMC/G4 and also higher than those for any reported Mg electrolytes (*20, 31*). The observed fast electrode kinetics is consistent with the improved overall bulk transport properties of the electrolyte solution. Galvanostatic cycling was conducted in Mg|

Mg symmetric cells (100 cycles, 1 C cm^{-2}) at four different current density values (1, 5, 10, and 50 mA cm^{-2}) (fig. S9). While both electrolytes are capable of cycling at an intermediate current density of 1 mA cm^{-2}, the overpotential for MMC/(DME-G2) (±39 mV) is significantly lower than that of MMC/G4 (±97 mV). At high (10 mA cm^{-2}) and ultrahigh (50 mA cm^{-2}) current densities, the cell with MMC/(DME-G2) (fig. S9C) continues to cycle stably while that with MMC/G4 is incapable of cycling even at 10 mA cm^{-2} (fig. S9B). The excellent rate performance is confirmed in Mg|Cu asymmetric cells in Fig. 3E. Remarkably, even at 50 mA cm^{-2}, MMC/(DME-G2) enables Mg deposition/stripping with a CE of 99.7 %. The morphology of Mg deposited on Cu substrate at 20 mA cm^{-2} with areal capacity of 3 mAh cm^{-2} appears dense, smooth, and dendrite-free (Fig. 3F). A symmetric Mg|Mg cell cycling at the same condition remains stable after a cumulative capacity of 833 mAh cm^{-2} (Fig.3G), far greater than those used in previously reported Mg|Mg symmetric cells (table S4). Our results consolidate Mg metal as a safe anode for advanced batteries even under demanding conditions.

Coupling PTO cathode with MMC/(DME-G2) yields an ultrahigh-power Mg battery prototype. At a current density of 408 mA g^{-1} (1 C), two discharge plateaus become more obvious compared to cells with MMC/G4, and the average discharge voltage slightly increases to 2.1 V (Fig. 4A). Furthermore, the rate capability is improved significantly even at high current densities of 8.16 A g^{-1} (20 C) and 20.4 A g^{-1} (50 C), where specific capacities of 278 and 210 mAh g^{-1}, respectively, can be retained. Stable cycling at 2.04 A g^{-1} (5 C) for over 200 cycles with 82% capacity retention (Fig. 4B) is achieved. This stability is enabled by a GO/graphene nanoparticles (GN) membrane (fig. S3, C and D) with the necessary modification to simultaneously allow faster Mg^{2+} diffusion and confinement of soluble PTO intermediate (*32*). Future work on tailoring the physical/chemical properties of the membrane could result in enhanced intermediate trapping and better cycling stability. Finally, Fig. 4C compares the Ragone plot of state-of-art Mg batteries that store Mg^{2+}, therefore excluding batteries storing complex ions. Both intercalation-type cathodes (Mo_6S_8, Ti_2S_4) and conversion-type cathodes (S and I_2) based on solid-liquid reactions involving bond cleavage and re-formation display slow kinetics (up to 2 C). In contrast, our cathode material based on bond cleavage-free solid-liquid reactions demonstrate a record specific power of 30.4 kW kg^{-1}, a big stride from 0.44 kW kg^{-1}, the next highest power Mg battery (*15*), while still providing a high material-level specific energy of 313 Wh kg^{-1}.

In conclusion, we have developed an ultrafast Mg battery featuring an organic quinone cathode with a MMC/(DME-G2) electrolyte solution. The bond cleavage-free solid-liquid reactions hold the key to fast Mg^{2+} storage, and the highly conducting MMC electrolyte enables high-rate Mg plating in a dendrite-free fashion. Our results set new directions for developing high-performance Mg cathode materials and electrolyte solutions, and unearth new possibilities of using energy-dense metals for fast energy storage.

References and Notes

1. H. D. Yoo *et al.*, Mg rechargeable batteries: an on-going challenge. *Energy Environ. Sci.* **6**, 2265-2279 (2013).
2. J. W. Choi, D. Aurbach, Promise and reality of post-lithium-ion batteries with high energy densities. *Nat. Rev. Mater.* **1**, 16013 (2016).

3. L. Suo *et al.*, "Water-in-salt" electrolyte enables high-voltage aqueous lithium-ion chemistries. *Science* **350**, 938 (2015).
4. R. Attias, M. Salama, B. Hirsch, Y. Goffer, D. Aurbach, Anode-electrolyte interfaces in secondary magnesium batteries. *Joule* **3**, 27-52 (2019).
5. R. Mohtadi, F. Mizuno, Magnesium batteries: Current state of the art, issues and future perspectives. *Beilstein J. Nanotechnol.* **5**, 1291-1311 (2014).
6. L. F. Wan, B. R. Perdue, C. A. Apblett, D. Prendergast, Mg desolvation and intercalation mechanism at the Mo_6S_8 chevrel phase surface. *Chem. Mater.* **27**, 5932-5940 (2015).
7. P. Canepa *et al.*, Odyssey of multivalent cathode materials: open questions and future challenges. *Chem. Rev.* **117**, 4287-4341 (2017).
8. X. Sun *et al.*, A high capacity thiospinel cathode for Mg batteries. *Energy Environ. Sci.* **9**, 2273-2277 (2016).
9. H. Dong *et al.*, Directing Mg-storage chemistry in organic polymers toward high-energy Mg batteries. *Joule* **3**, 782-793 (2019).
10. Z. Li *et al.*, Fast kinetics of multivalent intercalation chemistry enabled by solvated magnesium-ions into self-established metallic layered materials. *Nat. Commun.* **9**, 5115 (2018).
11. H. D. Yoo *et al.*, Fast kinetics of magnesium monochloride cations in interlayer-expanded titanium disulfide for magnesium rechargeable batteries. *Nat. Commun.* **8**, 339 (2017).
12. H. Kim *et al.*, Sodium intercalation chemistry in graphite. *Energy Environ. Sci.* **8**, 2963-2969 (2015).
13. T. Gao *et al.*, Reversible S_0/MgS_x redox chemistry in a $MgTFSI_2/MgCl_2$/DME electrolyte for rechargeable Mg/S batteries. *Angew. Chem. Int. Ed.* **56**, 13526-13530 (2017).
14. X. Yu, A. Manthiram, Performance enhancement and mechanistic studies of magnesium–sulfur cells with an advanced cathode structure. *ACS Energy Lett.* **1**, 431-437 (2016).
15. A. Du *et al.*, An efficient organic magnesium borate-based electrolyte with non-nucleophilic characteristics for magnesium–sulfur battery. *Energy Environ. Sci.* **10**, 2616-2625 (2017).
16. H. Yamin, Lithium sulfur battery. *J. Electrochem. Soc.* **135**, 1045 (1988).
17. M. V. Merritt, D. T. Sawyer, Electrochemical reduction of elemental sulfur in aprotic solvents. Formation of a stable S_8- species. *Inorganic Chemistry* **9**, 211-215 (1970).
18. D. Aurbach *et al.*, Prototype systems for rechargeable magnesium batteries. *Nature* **407**, 724-727 (2000).
19. O. Tutusaus *et al.*, An efficient halogen-free electrolyte for use in rechargeable magnesium batteries. *Angew. Chem. Int. Ed.* **54**, 7900-7904 (2015).
20. Z. Zhao-Karger, M. E. Gil Bardaji, O. Fuhr, M. Fichtner, A new class of non-corrosive, highly efficient electrolytes for rechargeable magnesium batteries. *J. Mater. Chem. A* **5**, 10815-10820 (2017).
21. Y. Shao *et al.*, Nanocomposite polymer electrolyte for rechargeable magnesium batteries. *Nano Energy* **12**, 750-759 (2015).
22. N. N. Rajput, T. J. Seguin, B. M. Wood, X. Qu, K. A. Persson, Elucidating solvation structures for rational design of multivalent electrolytes—A review. *Topics Curr. Chem.* **376**, 19 (2018).

23. X. Huang *et al.*, Cyclic voltammetry in lithium–sulfur batteries—challenges and opportunities. *Energy Technol.* **7**, 1801001 (2019).
24. T. Suga, Y.-J. Pu, K. Oyaizu, H. Nishide, Electron-transfer kinetics of nitroxide radicals as an electrode-active material. *Bull. Chem. Soc. Jpn.* **77**, 2203-2204 (2004).
25. M. Martínez-Cifuentes, R. Salazar, O. Ramírez-Rodríguez, B. Weiss-López, R. Araya-Maturana, Experimental and theoretical reduction potentials of some biologically active ortho-carbonyl para-quinones. *Molecules* **22**, 577 (2017).
26. Y.-C. Lu, Q. He, H. A. Gasteiger, Probing the lithium–sulfur redox reactions: A rotating-ring disk electrode study. *J. Phys. Chem. C* **118**, 5733-5741 (2014).
27. J.-Q. Huang *et al.*, Permselective graphene oxide membrane for highly stable and anti-self-discharge lithium–sulfur batteries. *ACS Nano* **9**, 3002-3011 (2015).
28. M. Salama *et al.*, On the feasibility of practical Mg–S batteries: practical limitations associated with metallic magnesium anodes. *ACS Appl. Mater. Interfaces* **10**, 36910-36917 (2018).
29. R. K. Harris, E. D. Becker, S. M. Cabral de Menezes, R. Goodfellow, P. Granger, NMR nomenclature: nuclear spin properties and conventions for chemical shifts: IUPAC recommendations 2001. *Solid State Nucl. Magn. Reson.* **22**, 458-483 (2002).
30. B. D. Adams, J. Zheng, X. Ren, W. Xu, J.-G. Zhang, Accurate determination of coulombic efficiency for lithium metal anodes and lithium metal batteries. *Adv. Energy Mater.* **8**, 1702097 (2018).
31. J. Luo, Y. Bi, L. Zhang, X. Zhang, T. L. Liu, A stable, non-corrosive perfluorinated pinacolatoborate Mg electrolyte for rechargeable Mg batteries. *Angew. Chem. Int. Ed.* **58**, 6967-6971 (2019).
32. W. Wang *et al.*, Graphene oxide membranes with tunable permeability due to embedded carbon dots. *Chem. Commun.* **50**, 13089-13092 (2014).

Acknowledgments

Funding: Y.Y. acknowledges the funding support from the U.S. Department of Energy's Office of Energy Efficiency and Renewable Energy (EERE), as part of the Battery 500 Consortium DE-EE0008234. This research used resources of the Advanced Light Source, which is a DOE Office of Science User Facility under contract no. DE-AC02-05CH11231. RM, OT are grateful for Dr. Koji Suto, Mr. Yukinari Kotani, Dr. Fuminori Mizuno, Dr. Tomoya Matsunaga from Toyota Motor Corporation and Dr. Kensuke Takechi from Toyota Central R&D for the support and very helpful discussions. They are also thankful to Mr. Ryuta Sugiura and Mr. Toshihiko Inoue at Toyota Research Institute of North America for the insightful information. R.M. and O.T. acknowledges the project's funding provided from Toyota Motor Corporation. **Author contributions:** H.D., O.T., Y.L, R.M. and Y.Y. conceived the concept and designed the experiments. R.M. and Y.Y. supervised the project. O.T. and R.M. synthesized the electrolytes. H.D. synthesized and fabricated organic electrodes. H.D., O.T., and Y.Z. performed electrochemical and materials characterizations. H.D. and Y.Z. prepared GO membranes. W.Y. and Z.H. performed soft X-ray absorption spectroscopy measurements. H.D., O.T., Y.L., R.M. and Y.Y. wrote the manuscript. All authors commented on the results and the manuscript. **Competing interests:** The authors declare no competing interests. **Data and materials**

availability: All data are available in the manuscript or the supplementary materials. Correspondence and requests for materials should be addressed to corresponding authors R.M. or Y.Y.

Supplementary Materials:

Materials and Methods

Figs. S1 to S10

Supplementary Text

Tables S1 to S4

References (33-43)

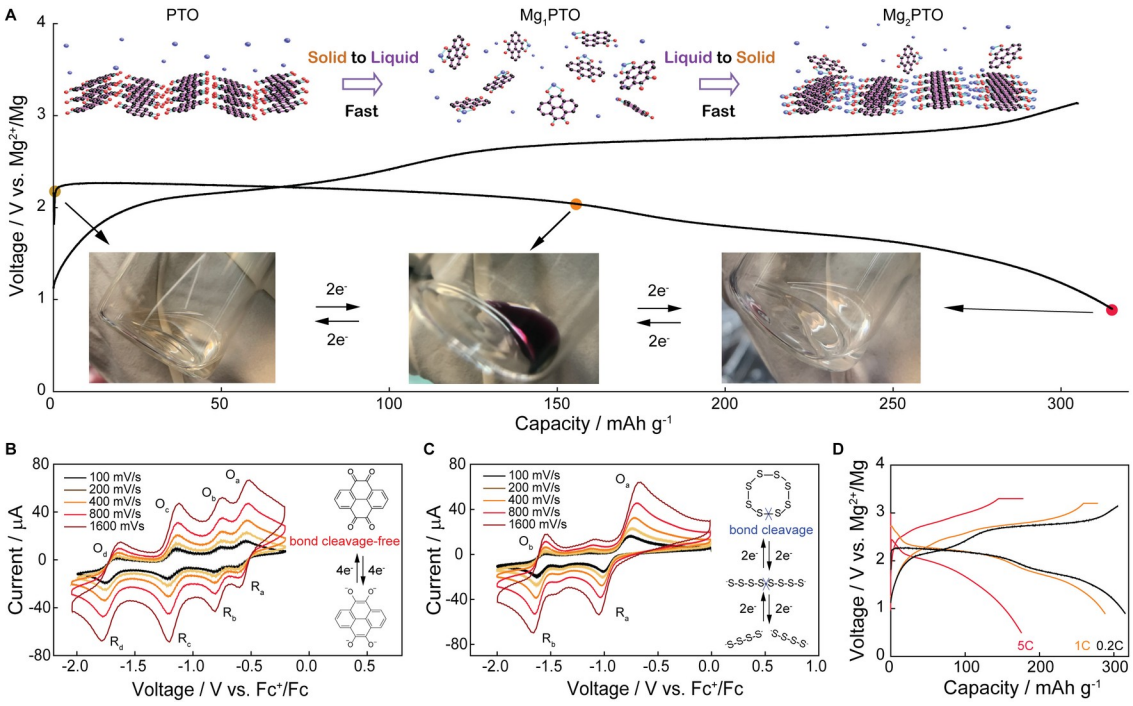

Fig. 1. A bond cleavage-free solid-liquid reaction. (A) Galvanostatic voltage profile of an Mg-PTO cell with MMC/G4 at 0.2 C (1 C = 408 mA g^{-1}). Inset shows the schematic of a solid-liquid-solid reaction during discharge. PTO electrodes at different states of discharge (open circuit voltage, half-discharged, and full-discharged) were extracted from the Swagelok cells and quickly submerged in DME solvents for three minutes to show solution color. **(B and C)** Cyclic voltammograms of 0.5 mM PTO (B) and S_8 (C) in a three-electrode setup using 0.1M tetra-n-butylammonium perchlorate acetonitrile solution. **(D)** Rate performance of Mg-PTO cells at 0.2, 1 and 5 C. Cells were tested under constant current-constant voltage (CC-CV) charging and constant current (CC) discharging modes; CV terminates when current decays to 0.2 C.

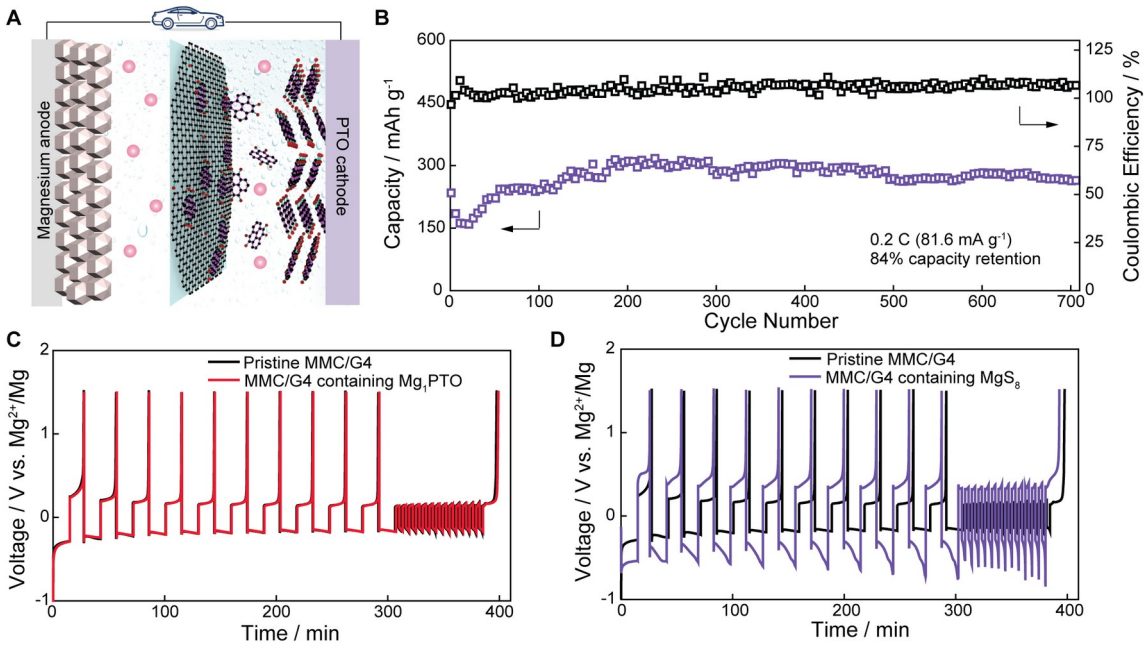

Fig. 2 Schematic of cell configuration with a thin graphene oxide (GO) membrane and Mg plating behavior in MMC/G4 electrolytes with and without trace amounts of soluble intermediates. (A) Schematic of a Mg-PTO cell with a thin (~2 μm) and light-weight (0.48 mg cm^{-2}) GO membrane to mitigate the dissolution of Mg_1PTO intermediate in electrolyte. **(B)** Cycling stability and coulombic efficiency of a GO-incorporated Mg-PTO cell cycled at the current density of 0.2 C (1 C = 408 mA g^{-1}). See fig. S5 for voltage profiles of the 1st, 2nd, 300th, 500th, and 700th cycle. The average coulombic efficiency slightly above 100 % could be ascribed to the imperfect confinement of soluble PTO intermediate by the GO membrane. **(C and D)** Voltage profiles of Mg|Cu asymmetric cells in pristine MMC/G4 electrolytes and that containing Mg_1PTO (C) or MgS_8 (D), respectively.

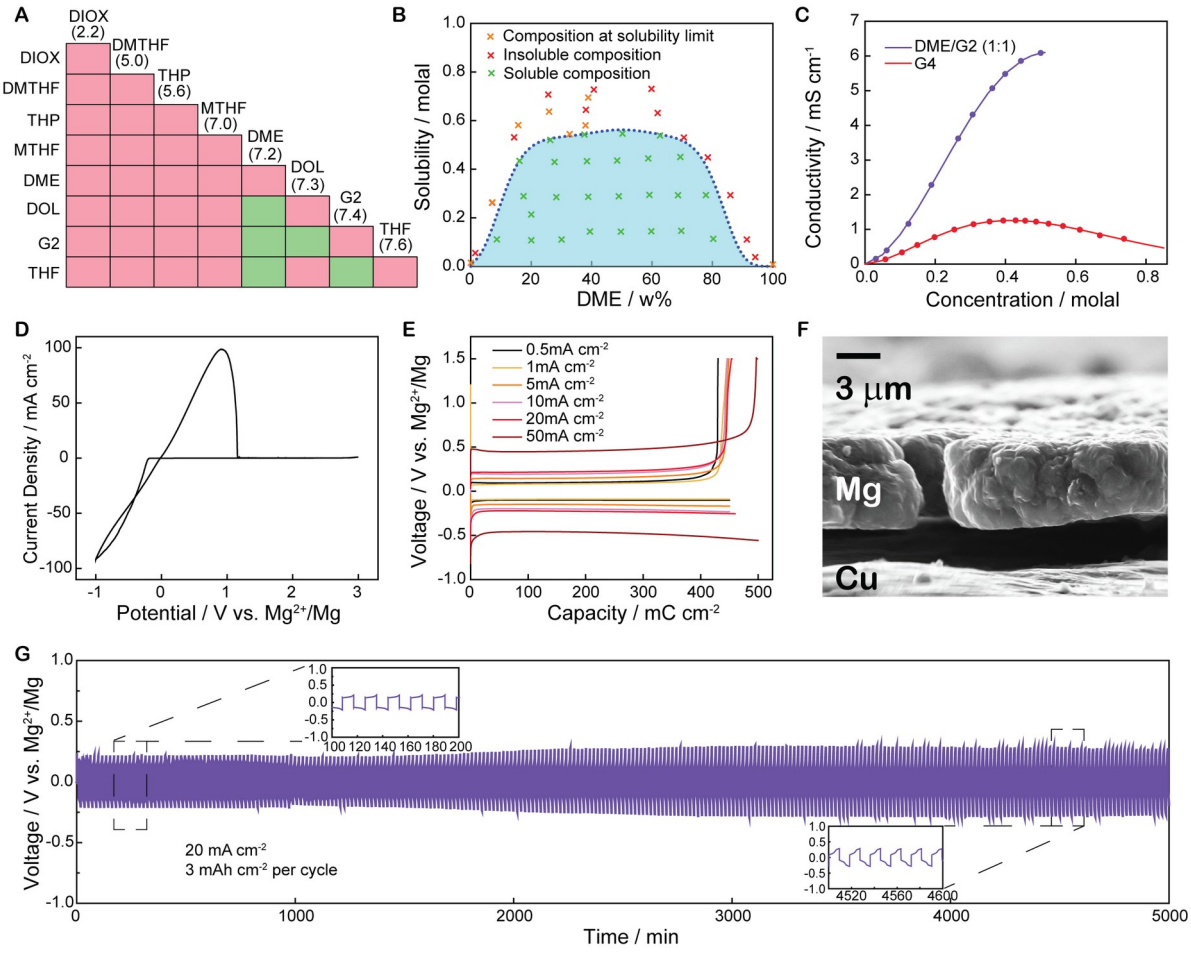

Fig. 3 Electrochemical performance of MMC/(DME-G2) electrolyte solutions. **(A)** Solubility chart of MMC at 0.3 *m* level in 1:1 (v/v) ethereal solvent blends (dielectric constants in parenthesis). Color code stands for solubility of MMC: pink (insoluble) and green (soluble). DIOX: 1,4-dioxane; DMTHF: 2,5-dimethyltetrahydrofuran; THP: tetrahydropyran; MTHF: 2-methyltetrahydrofuran; DME: 1,2-dimethoxyethane; DOL: 1,3-dioxolane; G2: diglyme; THF: tetrahydrofuran. **(B)** Solubility diagram of MMC in the mixture of DME/G2. **(C)** Ionic conductivity dependence on concentration of MMC solutions in G4 and DME/G2 mixture at 25°C. **(D)** Selected cyclic voltammogram for MMC/(DME-G2) on a Pt electrode at a scan rate of 35 mV s^{-1}. **(E)** Polarizations of a Mg|Cu asymmetric cell at current densities from 0.5 to 50 mA cm^{-2}. **(F)** Cross-sectional SEM image of Mg plated on a Cu substrate. **(G)** Galvanostatic voltage profiles of an Mg|Mg symmetric cell cycled at a current density of 20 mA cm^{-2} for plating (3 mAh cm^{-2}) and stripping (3 mAh cm^{-2}) per cycle for 5000 minutes.

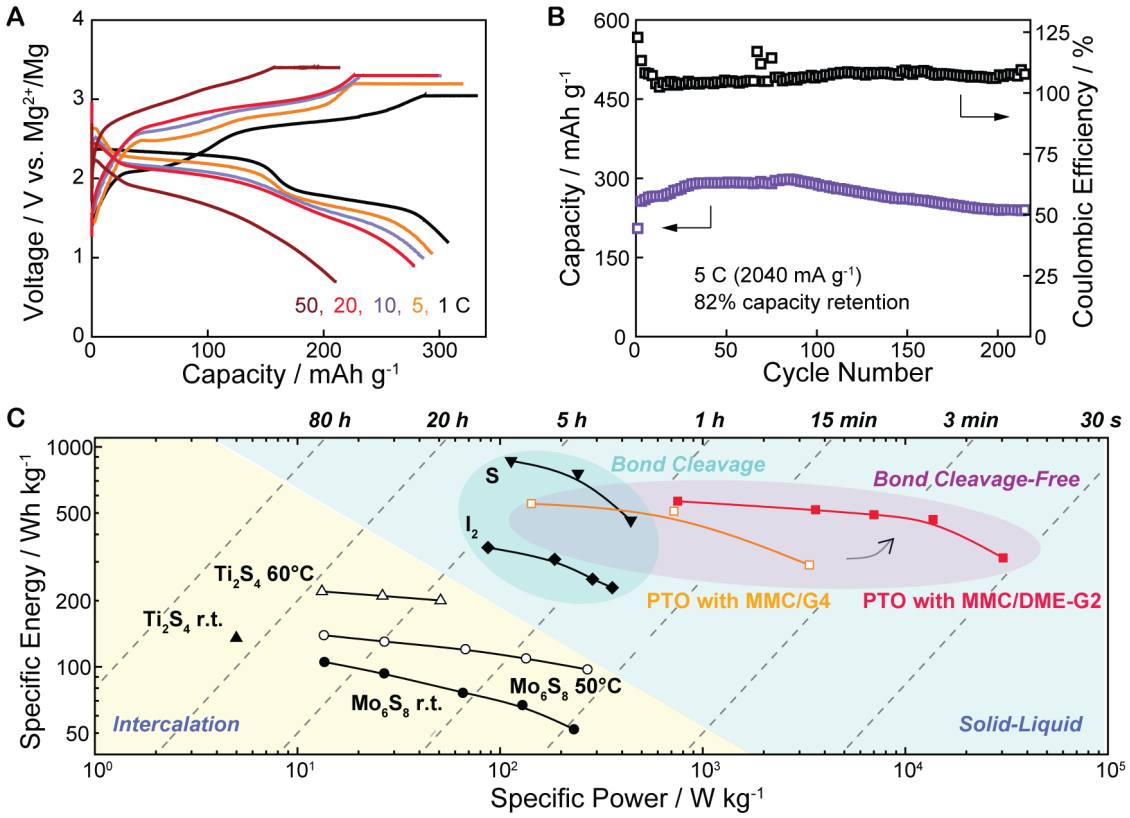

Fig. 4 Electrochemical performances of Mg-PTO batteries with MMC/(DME-G2) electrolyte solutions. **(A)** Voltage profiles of Mg-PTO cells at 1 to 50 C (1 C = 408 mA g^{-1}) using constant current-constant voltage (CC-CV) charging and constant current (CC) discharging modes. CC-CV terminated when current density decayed to 0.5 C. **(B)** Cycling stability and coulombic efficiency of a GO/GN-incorporated Mg-PTO cell cycled at 5 C. See fig. S10 for voltage profiles of the 1st, 2nd, 100th, and 200th cycle. The average coulombic efficiency slightly above 100 % could be ascribed to the imperfect confinement of soluble PTO intermediate by the GO/GN membrane. **(C)** Ragone plot of state-of-the-art Mg batteries that store pure Mg^{2+}. Calculation is based on the mass of cathode and anode active materials. The detailed parameters are summarized in table S1.